Full Paper Transactions, SMiRT 28
Toronto, Canada, August 10-15, 2025

FAILURE CRITERIA FOR SLOPE STABILITY ASSESSMENT USING DYNAMIC NONLINEAR ANALYSIS AND EFFECTS OF SUPPORT

Masataka Sawada[1], Nanami Sakamoto[2], Makoto Ishimaru[3], Yasuyuki Maeda[4], Tomoaki Suzuki[5], Hitoshi Tokunaga[6]

[1] Senior Research Scientist, Central Research Institute of Electric Power Industry, Abiko, Japan (sawada@criepi.denken.or.jp)
[2] Stuff Engineer, West Japan Engineering Consultants, Inc., Fukuoka, Japan (na-sakamoto@wjec.co.jp)
[3] Senior Research Scientist, Central Research Institute of Electric Power Industry, Abiko, Japan (ishimaru@criepi.denken.or.jp)
[4] Engineer, Ark Information Systems, Inc., Tokyo, Japan (maeda.yasuyuki@ark-info-sys.co.jp)
[5] Technical Manager, Ark Information Systems, Inc., Tokyo, Japan (suzuki.tomoaki@ark-info-sys.co.jp)
[6] Manager, Kyushu Electric Power Co., Inc., Fukuoka, Japan (Hitoshi_Tokunaga@kyuden.co.jp)

ABSTRACT

A method for evaluating the stability of slopes around important nuclear facilities using dynamic nonlinear analysis is being investigated. To put this method into practical use, it is necessary to establish a method for setting indicators and their threshold values for judging slope collapse. A dynamic nonlinear analysis of the seismic response of a virtual hard-rock slope with anchor reinforcement was conducted to investigate the effectiveness of multiple indicators for judging slope collapse. In cases without anchors, the time when the slip displacement increases rapidly is consistent with the time when the elements that exceed the failure shear strain are connected in series, as well as the time when the force of gravity on the slip surface significantly exceeds the resistance force. In cases with anchors, the time when the slip displacement rapidly increases is delayed owing to the effect of the anchors. Therefore, it is important to evaluate the soundness of the anchors to evaluate the stability of slopes reinforced with anchors.

INTRODUCTION

Recently, the need to evaluate the stability of rock slopes around critical structures during large earthquakes has increased. In particular, avoiding the collapse of the slopes around critical facilities in nuclear power plants due to earthquakes is necessary to maintain the safety functions of these facilities.

In Japan, a slip safety factor based on an equivalent linear analysis is conventionally used to evaluate the stability of rock slopes in terms of sliding motion during earthquakes (JEAG 4601-1987, 1987). However, a slip safety factor of less than 1.0 does not always correspond to a slope collapse (Ishimaru and Kawai, 2011). Therefore, evaluating seismic stability using ground displacement is considered a more effective approach. Shinoda et al. (2015) and Kawai et al. (2017) proposed methods that consider ground displacement for evaluating the stability of rock slopes.

Ishimaru et al. (2018) proposed a nonlinear analysis method that considers progressive failure to evaluate the stability of rock slopes, including post-earthquake residual displacement. They applied this method to a dynamic centrifuge model test. Their research demonstrated that the nonlinear analysis was relatively conservative, as it yielded a residual displacement slightly larger than that observed during the model test. However, criteria regarding the degree of deformation required to determine whether a slope is unstable have not yet been established. This is crucial for evaluating slope stability from deformation via nonlinear analysis.

Sawada et al. (2024) conducted seismic response analyses of a centrifuge slope model test and a virtual soft-rock slope. They proposed a method of conducting a preliminary seismic response analysis using periodic waves to establish a threshold for slip displacement, and then conducting the main seismic response analysis using input waves for evaluation.

In this paper, we report the results of a dynamic nonlinear analysis of a virtual hard-rock slope, as well as a study on the indicators and their threshold settings for judging slope collapse. Particular attention was given to the reinforcement effect of anchors and the effectiveness of using anchor soundness as an indicator of slope collapse.

NONLINEAR ANALYSIS METHOD

In dynamic nonlinear analyses, the effects of rock shear and tensile failures must be considered. Wakai et al. (2010) proposed an elastoplastic constitutive model that considered strain-softening characteristics and performed a dynamic finite element analysis of earthquake-induced landslides. Ishimaru et al. (2018) proposed a constitutive model that considered the influence of rock failure on the shear stress–shear strain relationship derived from the multiple shear spring model (Towhata and Ishihara, 1985) in a two-dimensional plane strain state. In this study, we used a constitutive model with modified post-failure equations (Ishimaru et al., 2019). The multiple shear spring model can consider anisotropy if the rigidity and strength are provided for each spring. However, isotropy was assumed in this study.

Constitutive Model of Material before Failure

The shear stress–shear strain curve before rock failure was modelled using the general hyperbolic equation (GHE) model (Tatsuoka and Shibuya, 1992), as expressed in Eq. (1). The GHE model can be fitted to experimental results over a wide strain range.

$$\tau = \frac{G_0 \cdot \gamma}{\frac{1}{C_1(\gamma)} + \frac{1}{C_2(\gamma)} \cdot \frac{|\gamma|}{\gamma_r}}. \tag{1}$$

Here, τ is the shear stress, γ is the shear strain, G_0 is the initial shear modulus, γ_r is the reference shear strain ($\gamma_r = \tau_{a0}/G_0$), and τ_{a0} is the initial reference shear strength. $C_1(\gamma)$ and $C_2(\gamma)$ are correction coefficients expressed as follows:

$$C_1(\gamma) = \frac{C_1(0)+C_1(\infty)}{2} + \frac{C_1(0)-C_1(\infty)}{2} \cdot \cos\left\{\frac{\pi}{\alpha/(|\gamma|/\gamma_r)+1}\right\}, \tag{2a}$$

$$C_2(\gamma) = \frac{C_2(0)+C_2(\infty)}{2} + \frac{C_2(0)-C_2(\infty)}{2} \cdot \cos\left\{\frac{\pi}{\beta/(|\gamma|/\gamma_r)+1}\right\}, \tag{2b}$$

where $C_1(0)$, $C_2(0)$, $C_1(\infty)$, $C_2(\infty)$, α, and β are parameters. The damping characteristics are assumed to conform to the model given in Eq. (3), which uses a virtual shear stress–shear strain curve (Ishihara et al., 1985) and the maximum damping constant h_{max}.

$$h = h_{max} \cdot (1 - G_R/G_0)^{\beta_1}. \tag{3}$$

Here, G_R is the shear modulus at the strain level of the unloading point, and β_1 is the adjustment parameter of the damping characteristics. The method proposed by Ozutsumi and Iai (2001) was used to set the damping constant in the multiple shear spring model.

Definitions of Strength and Failure

The shear strength is defined by Eq. (4) (compression is herein defined as positive).

$$\tau_f = c_p \cdot cos\phi_p + \frac{\sigma_1+\sigma_3}{2} \cdot sin\phi_p, \tag{4}$$

where τ_f is the peak shear strength, c_p is the peak cohesion, and ϕ_p is the peak internal friction angle. In addition, σ_1 is the maximum principal stress and σ_3 is the minimum principal stress. The shear failure was determined using Eq. (5a), and the tensile failure was determined using Eq. (5b), where σ_t is the tensile strength.

$$(\sigma_1 - \sigma_3)/2 \geq \tau_f, \tag{5a}$$

$$\sigma_3 \leq \sigma_t. \tag{5b}$$

Constitutive Model of Material after Failure

The shear stress–shear strain curve after rock failure also conforms to the GHE model, as shown in Eq. (1). However, the reference shear strain $\gamma_r = \tau_a/G_0$, and the reference shear strength τ_a decreases from the initial value τ_{a0} to the residual shear strength τ_r according to Eq. (6).

$$\tau_a = \tau_r + \frac{\tau_{a0}-\tau_r}{A \cdot \gamma^p + 1}. \tag{6}$$

Here, γ^p is the maximum absolute value of the shear strain (incremental amount from the value at failure) and A is the strain-softening coefficient, which is a parameter that determines the rate at which the reference shear strength decreases. Eq. (7) was used for the residual strength τ_r.

$$\tau_r = c_r \cdot cos\phi_r + \frac{\sigma_1+\sigma_3}{2} \cdot sin\phi_r, \tag{7}$$

where c_r is the residual cohesion and ϕ_r is the residual internal friction angle. The damping characteristics after failure are assumed to be the same as those in Eq. (3). However, the analysis program was modified such that additional damping H_f could be incorporated into Eq. (3).

When the tensile stress exceeds the tensile strength, the Mohr circle changes until the minimum principal stress reaches zero, while the maximum principal stress is maintained. The associated residual force is then distributed to the surrounding elements.

SIMULATION

In this study, we performed a dynamic nonlinear analysis of a virtual hard-rock slope with anchor installations. Based on the analysis results, we attempted to develop a method for setting the stability criteria in a nonlinear analysis of the ground by focusing on the continuous increase in displacement, continuation of large-strain elements, and other factors.

Simulation Model

The slope model used in this study is presented in Fig. 1. The slope height is 96.6 m. Regarding the boundary conditions in the seismic response analysis, the bottom was set as a viscous boundary, and the sides were also set as viscous boundaries with free ground to consider the notch forces.

The ground is divided into four layers according to rock mass classification. C_H, C_M, C_L, and D in Fig. 1 indicate the rock mass grade of each layer, with C_H representing the highest and D the lowest. This notation for rock mass grades is used in Japan and is associated with the deformation coefficients and strength constants of rock masses. A total of 13 anchors are set on the slope. The anchorage length is 10 m. The free lengths are 40 m for the top anchor and 30 m for the other anchors. We modelled the anchors using nonlinear truss elements. Each anchor consists of five tendons, and the anchorage points differ among the tendons. Anchor tension forces were applied at the five anchorage nodes and the surface nodes around the anchor head.

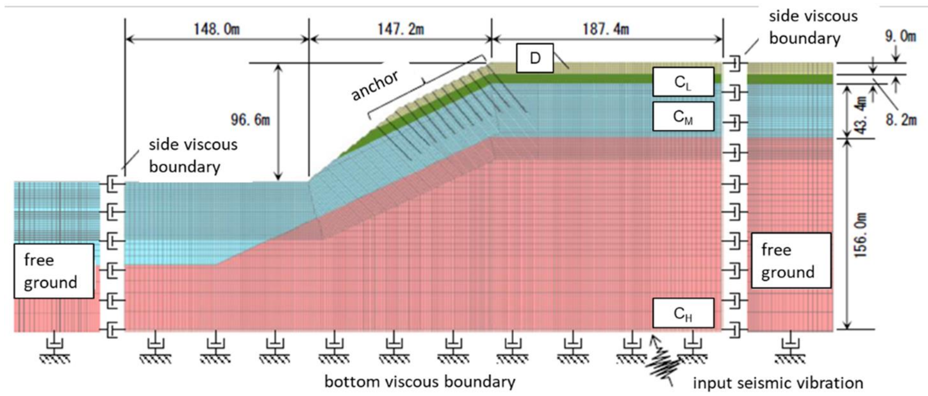

Figure 1. Hard-rock slope model with boundary conditions. C_H, C_M, C_L, and D indicate the rock mass grade of each layer, with C_H being the highest grade.

Table 1 lists the basic physical properties and strength of each rock mass grade. The strain dependencies of G and h before failure were considered only for the D-grade rock. The parameter values of the nonlinear constitutive model for the D-grade rock are listed in Table 2. The C_L-, C_M-, and C_H-grade rocks were set as linear elastic bodies before failure. We considered the failure effect for the D-, C_L-, and C_M-graded rocks and set the parameters based on the assumption that the shear stress immediately decreased to the residual strength after shear failure. However, we assumed that the shear strength was maintained after tensile failure. Even if a fracture disengages under tensile stress conditions, it is considered to reengage when the stress condition returns to compressive stress.

Table 1. Physical properties of each layer

Property	**D**	**C_L**	**C_M**	**C_H**
Wet unit weight γ_t (kN/m^3)	20	23	25	26
Initial shear modulus G_0 (kN/m^2)	500	3300	8100	11000
Poisson's ratio ν	0.43	0.40	0.37	0.35
Cohesion (peak) c_p (kN/m^2)	100	300	1000	-
Internal friction angle (peak) ϕ_p (degrees)	20	33	45	-
Cohesion (residual) c_r (kN/m^2)	0	0	0	-
Internal friction angle (residual) ϕ_r (degrees)	20	33	45	-
Tensile strength σ_t (kN/m^2)	0	0	0	-
Strain softening coefficient A	1.0×10^{15}	1.0×10^{15}	1.0×10^{15}	-
Damping ratio h_0	*	0.03 **	0.03 **	0.02 **
Additional damping ratio after failure H_f	0.1	0.1	0.1	-

* Eq (3) is used. See Table 2.

** Considered in stiffness-proportional form as damping ratio for the first-order natural frequency

Table 2. Physical properties regarding nonlinear constitutive model for D-grade rock layer.

Property	**D**
Reference shear strain γ_r	3.33×10^{-3}
Initial reference shear stress τ_{a0} (kN/m^2)	$\gamma_r \times G_0$
GHE model: $C_1(0), C_2(0)$	0.970, 0.340
$C_1(\infty), C_2(\infty)$	0.099, 1.347
α, β	0.299, 0.319
Maximum damping constant h_{max}	0.173
Adjustment parameter of the damping chracteristics β_1	2.0

Table 3 presents the physical properties of the anchors. We employed a trilinear kinematic-hardening model as a nonlinear material model for the anchor tendons, considering the yielding and breakage of the anchor tendons. A tensile force of 1000 kN was applied to each anchor. Note that the anchors were assumed to be cast at 2 m intervals in the depth direction, and the cross-sectional area in Table 3 and the aforementioned tension force were multiplied by one-half in this simulation model, which considered unit depth.

Table 3. Physical properties of anchors

Property	Value
Unit weight (kN/m^3)	1.94×10^5
Young's modulus of tendon (MN/m^2)	76.98
Cross-sectional area of all tendons (m^2)	1.387×10^{-3}
First yield strain	6.50×10^{-3}
Second yield strain	9.66×10^{-3}
Rigidity rate after the first yield strain	0.365
Rigidity rate after the second yield strain	0.050

First, a self-weight analysis was performed to obtain the stresses before the anchors were installed. In the case where anchors were installed, the results of the self-weight analysis were followed by a static analysis in which anchor tension forces were applied as nodal forces to the anchor heads and anchorage points. For the boundary conditions, we fixed the displacements at the bottom and applied vertical rollers at the sides. However, to prevent tensile failure due to the influence of the lateral boundaries, the self-weight analysis and nodal force loading analysis used a model that extended the analysis domain shown in Fig. 1 by approximately 200 m to the left and right. The obtained stresses were used as the initial conditions for the seismic response analysis.

Two types of waves, periodic and random, were used as input earthquake ground motions (see Fig. 2). The periodic wave was assumed to be used in the preliminary analysis, and the random wave was assumed to be used in the main analysis for evaluation. The periodic wave was a sinusoidal wave with a frequency of 1 Hz, with a 20-wave main part and a 4-wave taper before and after the main part. The acceleration was increased in steps of 1.0 m/s^2 from the first step d01, with a maximum acceleration of 2.0 m/s^2 to identify the vibration step leading to slope collapse. The direction of shaking was strictly horizontal. As the amplitude was progressively increased, the final state of the previous step was taken as the initial state of the next step; that is, the past stress and strain history was used. The random wave applied horizontal and vertical motion, and the analysis was performed with simultaneous shaking in both directions. The maximum acceleration of the horizontal motion was 6.0 m/s^2 and that of the vertical motion was 4.5 m/s^2. If the slope did not collapse, the amplitude of the input earthquake motion was doubled and then tripled. In this case, however, the past stress and strain history was not applied.

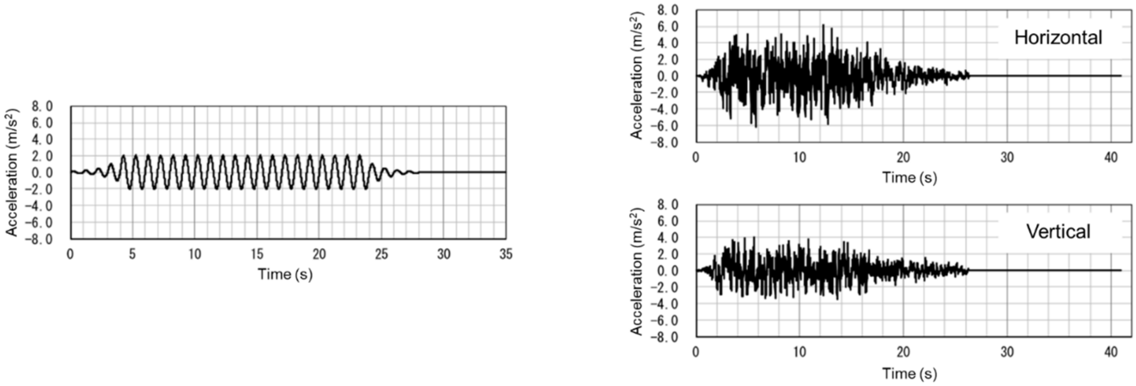

(a) Periodic wave (d01)　　(b) Random wave (x1)

Figure 2. Input waves

We conducted four simulations combining two types of input seismic waves, with and without anchors. In Cases 1 and 2, periodic and random waves, respectively, were input without anchors. In Cases 3 and 4, periodic and random waves, respectively, were input with anchors.

Table 4. Output items.

Type	Output
Countour	1. Maximum shear strain distribution (compared to failure shear strain) 2. Failure element distribution (tensile failure, shear failure, multiple failure)
Defomation	3. Deformation drawing
Time history	4. Displacement on slip surface 5. Normalized slip (= slip displacement / slip surface length) 6. Stability index F_d 7. The maximum value of shear strain across all elements 8. The number of failure elements 9. The number of elements where maximum shear strain exceeds the failure shear strain 10. The number of interations in each time step and residual force norm 11. Anchor tendon tension 12. Confining stress at the anchorage points

Results

The items in Table 4 were output with the aim of assessing the slope collapse on the basis of the simulation results. First, we focused on the occurrence of significant displacement and the continuation of displacement during the period when earthquake motion was not applied. The formation of a slip surface (a series of finite elements with a high maximum shear strain) and the spread of the failure elements were examined. The stability index F_d, proposed by Wakai et al. (2007), is defined as

$$F_d = \frac{\sum R_f}{\sum T_s}, \tag{8}$$

where $\sum T_s$ is the sliding force on the slip surface due to the weight of the sliding mass, and $\sum R_f$ is the maximum shear resistance force that can be exerted on the slip surface. The history of the maximum value of shear strain across all elements, number of elements that have experienced failure, and number of elements whose maximum shear strain exceeds a threshold value are representative of the computational domain without considering the location of the slip surface. Therefore, slope collapse can be judged relatively straightforwardly based on these histories. In the model considering anchors, the tension of the tendons and condition of the anchorage rock mass were checked. Based on the knowledge that the pullout force is retained with confining stress even if a crack exists in the anchorage body (Kobayakawa et al., 2023), the anchor was judged to be sound if a confining stress was acting in the direction perpendicular to the anchor axis, even if tensile failure occurred in the anchorage rock mass.

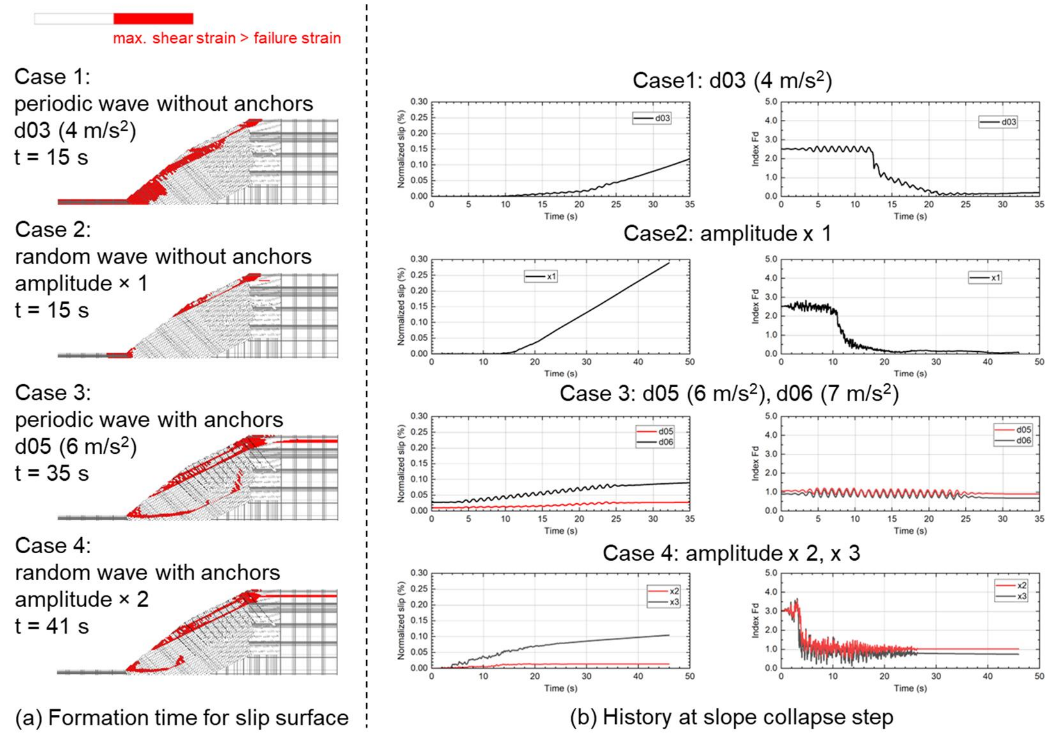

Figure 3. Formation of slip surface and time histories of normalized slip and index F_d at slope collapse step. (a) Elements whose maximum shear strain exceeds the failure strain are shown in red. At the steps and times shown in the figure, the elements in red were continuous and formed a slip surface. (b) In the cases with anchors, the formation of the slip surface does not necessarily coincide with slope collapse. Case 3 shows the history of the slip surface formation step and the following step; Case 4 shows the history obtained from a calculation using an input wave with doubled amplitude that formed the slip surface, as well as the history from a calculation using an even larger input wave with tripled amplitude.

In this study, a slope was considered to have collapsed when the following conditions were satisfied: 1) significant residual displacement occurred at the ground surface, 2) a series of elements with maximum shear strains exceeding the failure strain formed a slip surface, and 3) the index F_d for the formed slip surface was less than 1.0. Figure 3(a) shows the distribution of elements whose maximum shear strain exceeded the failure strain when the slip surface was considered to have formed in each case. In each case, a slip surface formed along the boundary between the D- and C_L- grade rock layers from the top of the slope. Figure 3(b) shows the histories of the normalized slip and the index F_d at the steps where the slope was evaluated as having collapsed. The normalized slip was calculated by dividing the relative displacement at the output node in the sliding block by the length of the slip surface. In Cases 1 and 2, the normalized slip began to increase after the slip surface was formed. In particular, the normalized slip increased rapidly after F_d fell below 0.5 and continued to increase after the seismic input ended. We determined that the slope collapsed immediately after the slip surface was formed in Cases 1 and 2. In contrast, Cases 3 and 4, in which anchors were installed, exhibited a different trend from that of Cases 1 and 2. In Case 3, the slip surface formed at step d05, and F_d was slightly below 1.0, but the normalized slip stopped increasing after the end of the seismic input. The anchors were considered to suppress the slip. In the next step, d06, the normalized slip continued after the end of the seismic input. We determined that the slope collapsed at this step. In Case 4, the input of random waves with twice the amplitude formed a slip surface, and F_d temporarily fell below 1.0; however, the increase in the normalized slip was limited. The increase in the normalized slip became more significant during the input of random waves with three times the amplitude and continued to increase even after the end of the seismic input. We determined that the slope collapsed not during the doubled input wave but during the tripled input wave.

Next, we examined the condition of the anchor. The anchor tendons did not yield during the steps shown in Fig. 3. Figure 4 shows the history of the stress perpendicular to the anchor axis acting on the rock at the anchorage. If the stress is on the compressive side, a confining pressure is considered to act on the anchorage, and the pullout load capacity is maintained. The results for Case 3 show that the stresses are stable on the compressive side at step d05, although they fluctuate in response to the seismic motion. However, in step d06, the stresses became unstable owing to shear failure of the rock at the anchorage. In Case 4, the stresses were stable on the compressive side for the doubled input wave but became unstable for the tripled input wave.

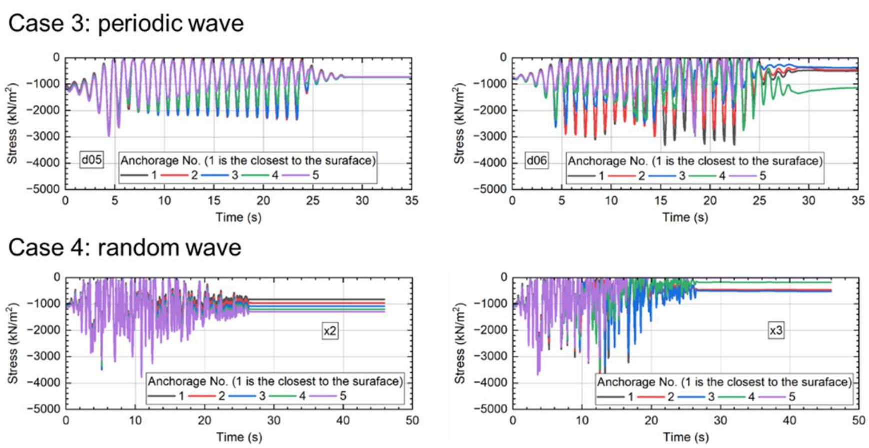

Figure 4. Confining stress progression at anchorage points.

Discussion

Based on our previous simulations (Sawada et al., 2024) and the simulations conducted in this study, we evaluated each output item as an indicator of slope collapse, as shown in Table 5. A rapid increase in slip displacement occurred immediately after the formation of the slip surface by a series of elements exhibiting strain values that exceeded the failure strain in the cases without anchors. The index F_d being below 1.0 indicates that the sliding force on the slip surface due to gravity exceeded the resistance, but the simulation showed a rapid increase in slip when F_d fell below approximately 0.5. In the cases with anchors, the formation of a slip surface did not cause a rapid increase in slip, and the value of F_d on the slip surface did not drop to 0.5. A rapid increase in slip was observed when the shear failure of the rock around the anchorage occurred.

Figure 5 shows the distribution of the maximum shear strain and displacement at the end of the step in which the slope was evaluated as having collapsed. If the anchor conditions are the same, the collapse modes are consistent regardless of whether the input seismic motion waves are periodic or random.

Table 5. Evaluation of each output item in terms of the slope stability criteria.

Output items	Usefulness
1. Maximum shear strain distribution (compared to failure shear strain)	+ +
2. Failure element distribution (tensile failure, shear failure, multiple failure)	+
3. Deformation drawing	+
4. Displacement on slip surface	+ +
5. Slip displacement / slip surface length	+ +
6. Stability index F_d	+ +
7. The maximum value of shear strain across all elements	+
8. The number of failure elements	–
9. The number of elements where maximum shear strain exceeds the failure shear strain	–
10. The number of interations in each time step and residual force norm	–
11. Anchor tendon tension	+ +
12. Confining stress at the anchorage points	+

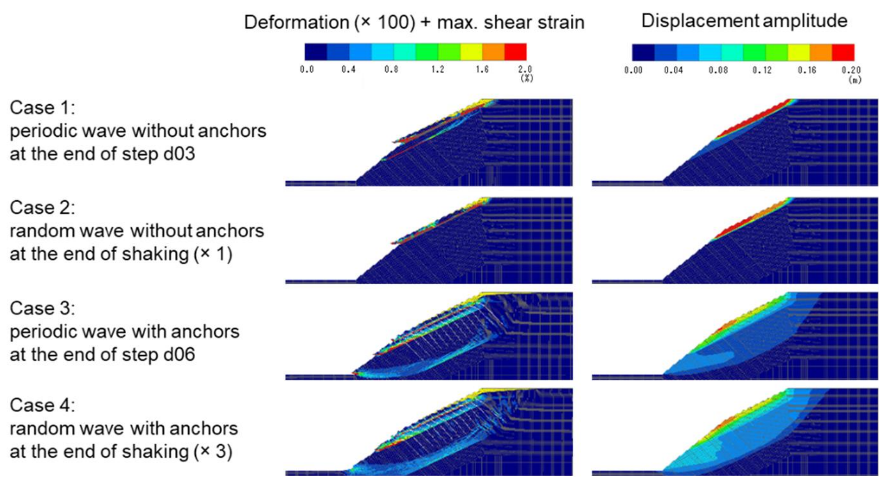

Figure 5. Contours of maximum shear strain with deformation and displacement amplitude. For deformation, the displacement is multiplied by 100.

The following method of setting the slope stability criteria is considered effective: 1) Conduct a preliminary analysis using periodic waves as the input seismic motion and set the indicators and their threshold values. 2) Conduct the main analysis using the input seismic motion for evaluation (usually random waves) and evaluate the slope stability based on the criteria set in 1). Concrete examples are provided as follows based on the slope model used in this study. If anchors are not considered, the steps that form the slip surface are identified in the preliminary analysis, and a slip threshold is set based on the rapid increase in slip and the value of F_d. For example, we can set the slip at the time when $F_d = 0.5$ as the threshold value. If anchors are considered, the formation of the slip surface, rapid increase in slip, value of F_d, and soundness of the anchors (tendon and anchorage) should be examined in the preliminary analysis. While the confining pressure acts on the anchorage, the slope is stable even if a slip surface is formed, and we can set the threshold to the slip at the time when the anchorage becomes unstable. However, it is desirable to develop a nonlinear model of the tendon pull-out behavior of the anchorage part and introduce it into the analysis program.

CONCLUDING REMARKS

The slip displacement threshold for slope collapse judgment can be set by referring to the following indicators after conducting a preliminary analysis. In cases without anchors, the threshold can be set based on the rapid increase in slip, the decrease in index F_d, and the formation of a slip surface. In cases with anchors, the soundness of the anchors must also be considered in addition to the above.

REFERENCES

Ishihara, K., Yoshida, N. and Tsujino, S. (1985). "Modelling of stress-strain relations of soils in cyclic loading," *Proc. 5th Int. Conf. Numerical Methods in Geomechanics*, Vol. 1, Nagoya, April 1-5, 373-380.

Ishimaru, M. and Kawai, T. (2011). "Basic study of the evaluation of seismic stability of rock slope using centrifuge model test," *Journal of Japan Society of Civil Engineers Ser. C*, 67(1), 36-49. (in Japanese)

Ishimaru, M., Okada, T., Nakamura, H., Kawai, T. and Kazama, M. (2017). "Modeling of strength and deformation characteristics after shear failure of soft rock and application to evaluation of seismic stability of slopes against sliding," *Journal of Japan Society of Civil Engineers Ser. C*, 73(1), 23-38. (in Japanese)

Ishimaru, M., Hashi, K., Oikawa, K. and Kawai, T. (2018). "Nonlinear analysis method for evaluating the seismic stability of rock slopes considering progressive failure," *Journal of Earthquake and Tsunami*, 12(4), 1841008 (16 pages).

Ishimaru, M, Sekiguchi, A., Okada, T. and Morozumi, H. (2019). "Numerical simulations on the seismic stability of rock foundations under critical facilities via dynamic nonlinear analysis," *Proc. 2019 Rock Dynamics Summit*, 658-663.

JEAG 4601-1987. (1987). *Technical Guidelines for Aseismic Design of Nuclear Power Plants*, Japan Electric Association, Japan.

Kawai, T., Oshima, T., Ishimaru, M. and Hashi, K. (2017). "Proposal for using ground displacement to evaluate the seismic stability of critical facilities' surrounding slopes and foundation ground," *Proc. 24th Int. Conf. Structural Mechanics in Reactor Technology*, Busan, Korea, August 20-25, Paper No. SS-02-01, 1-10.

Kobayakawa, H., Ishimaru, M. and Hiraga, K. (2023). "Pull-out tests on anchor models in artificial rock - Effect of confining pressure-," *Proceedings of 78th Annual Meeting of JSCE*, CS10-85. (in Japanese)

Ozutsumi, O. and Iai, S. (2001). "Adjustment method of the hysteresis damping for multiple shear spring model," *Proc. 4th Int. Conf. Recent Advances in Geotechnical Earthquake Engineering and Soil Dynamics*, Paper No. 1.68, San Diego, California, March 26-31, pp. 1-6.

Sawada, M., Sakamoto, N., Ishimaru, M., Maeda, Y., Suzuki, T. and Tokunaga, H. (2024). "Failure criteria for slope stability assessment using dynamic nonlinear analysis," *Transactions of the SMiRT27*, Yokohama, Japan.

Shinoda, M., Watanabe, K., Sanagawa, T., Abe, K., Nakamura, H., Kawai, T. and Nakamura, S. (2015). "Dynamic behavior of slope models with various slope inclinations," *Soils and Foundations*, 55(1), 127-142.

Tatsuoka, F. and Shibuya, S. (1992). "Deformation characteristics of soils and rocks from field and laboratory tests," *Proc. 9th Asian Regional Conf. Soil Mechanics and Foundation Engineering*, Vol. 2, Bangkok, Thailand, 101-170.

Towhata, I. and Ishihara, K. (1985). "Modelling soil behavior under principal stress axes rotation," *Proc. 5th Int. Conf. Numerical Method in Geomechanics*, 1, Nagoya, April 1-5, 523-530.

Wakai, A., Ugai, K., Onoue, A., Higuchi, K. and Kuroda, S. (2007). "Finite element simulation for collapse of dip slope during earthquake induced by strain-softening behavior of bedding plane," *Landslides*, 44(3), 145-155. (in Japanese)

Wakai, A., Ugai, K., Onoue, A., Kuroda, S. and Higuchi, K. (2010). "Numerical modeling of an earthquake-induced landslide considering the strain-softening characteristics at the bedding plane," *Soils and Foundations*, 50(4), 533-545.